



# Transformation of frequency-magnitude relation prior to large events in the model of block structure dynamics

A. Soloviev

## ► To cite this version:

A. Soloviev. Transformation of frequency-magnitude relation prior to large events in the model of block structure dynamics. *Nonlinear Processes in Geophysics*, 2008, 15 (1), pp.209-220. hal-00302971

**HAL Id: hal-00302971**

**<https://hal.science/hal-00302971>**

Submitted on 27 Feb 2008

**HAL** is a multi-disciplinary open access archive for the deposit and dissemination of scientific research documents, whether they are published or not. The documents may come from teaching and research institutions in France or abroad, or from public or private research centers.

L'archive ouverte pluridisciplinaire **HAL**, est destinée au dépôt et à la diffusion de documents scientifiques de niveau recherche, publiés ou non, émanant des établissements d'enseignement et de recherche français ou étrangers, des laboratoires publics ou privés.

# Transformation of frequency-magnitude relation prior to large events in the model of block structure dynamics

A. Soloviev

International Institute of Earthquake Prediction Theory and Mathematical Geophysics, Russian Academy of Sciences, Moscow, Russia

ESP, The Abdus Salam International Centre for Theoretical Physics, Trieste, Italy

Received: 2 July 2007 – Revised: 17 September 2007 – Accepted: 21 January 2008 – Published: 27 February 2008

**Abstract.** The  $b$ -value change in the frequency-magnitude (FM) distribution for a synthetic earthquake catalogue obtained by means of the model of block structure dynamics has been studied. The catalogue is divided into time periods preceding strong earthquakes and time periods that do not precede strong earthquakes. The separate analysis of these periods shows that the  $b$ -value is smaller before strong earthquakes. The similar phenomenon has been found also for the observed seismicity of the Southern California. The model of block structure dynamics represents a seismic region as a system of perfectly rigid blocks divided by infinitely thin plane faults. The blocks interact between themselves and with the underlying medium. The system of blocks moves as a consequence of prescribed motion of the boundary blocks and of the underlying medium. As the blocks are perfectly rigid, all deformation takes place in the fault zones and at the block base in contact with the underlying medium. Relative block displacements take place along the fault zones. Block motion is defined so that the system is in a quasistatic equilibrium state. The interaction of blocks along the fault zones is viscous-elastic (“normal state”) while the ratio of the stress to the pressure remains below a certain strength level. When the critical level is exceeded in some part of a fault zone, a stress-drop (“failure”) occurs (in accordance with the dry friction model), possibly causing failure in other parts of the fault zones. These failures produce earthquakes. Immediately after the earthquake and for some time after, the affected parts of the fault zones are in a state of creep. This state differs from the normal state because of a faster growth of inelastic displacements, lasting until the stress falls below some other level. This numerical simulation gives rise a synthetic earthquake catalogue.

Correspondence to: A. Soloviev  
(soloviev@mitp.ru)

## 1 Introduction

The study of seismicity with the statistical and phenomenological analysis of observed earthquake catalogues has the disadvantage that the reliable data cover, in general, a time interval of about one hundred years or even less. This time interval is very short, in comparison with the duration of tectonic processes responsible of the seismic activity. Therefore the patterns of the earthquake occurrence identifiable in the catalogue may be only apparent and may not repeat in the future. This can be overcome by numerical modelling of the processes generating seismicity and analyzing obtained synthetic earthquake catalogues that cover many seismic cycles and allow studying the dependence of seismicity on the model parameters.

Several models based on spring-block interaction, cellular automata, scaling organization of fracture tectonics, colliding cascades etc. (Burridge and Knopoff, 1967; Allègre et al., 1982, 1995; Bak and Tang, 1989; Olami et al., 1992; Blanter et al., 1998; Gabrielov et al., 2000) have been developed to reproduce general properties of observed seismicity. Other models have implemented specific mechanisms in the fault zone (e.g., Nur and Booker, 1972; Dieterich, 1972, 1994; Barenblatt, 1983; Gabrielov and Keilis-Borok, 1983; Ito and Matsuzaki, 1990; Hainzl et al., 1999; Ben-Zion and Lyakhovsky, 2006). These models reproduce certain observed phenomena but it is rather difficult to apply them to an actual fault system. This can be made by means of models that generate synthetic earthquake catalogues for a large heterogeneous strike-slip fault (Ben-Zion and Rice, 1993; Zöller et al., 2005) and for a system of faults (e.g., Ward, 1992, 2000; Robinson and Benites, 1996, 2001; Fitzenz and Miller, 2001; Zhou, 2006).

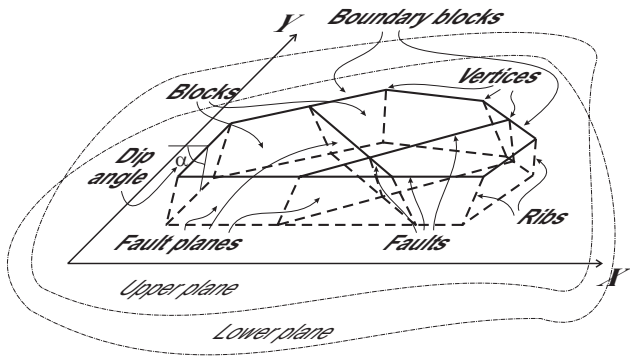


**Fig. 1.** On definitions used in the model of block structure dynamics.

The model of the block structure dynamics (Gabrielov et al., 1990; Keilis-Borok et al., 1997; Soloviev and Ismail-Zadeh, 2003) exploits the hierarchical block structure of the lithosphere. The model is based on the assumption that blocks of the lithosphere are separated by comparatively thin, weak and less consolidated fault zones, such as lineaments and tectonic faults. In a seismotectonic process major deformation and most earthquakes occur in such fault zones. Synthetic earthquakes are generated in the model as a result of movement of blocks creating stress in the fault zones. The model allows to reproduce the block structure of a region under consideration and has been applied to simulate block dynamics and seismicity of the real seismic regions (Soloviev and Ismail-Zadeh, 2003; Ismail-Zadeh et al., 2007).

A seismic region is modelled by a system of perfectly rigid blocks divided by infinitely thin plane faults. The blocks interact between themselves and with the underlying medium. The system of blocks moves as a consequence of prescribed motion of the boundary blocks and of the underlying medium. As the blocks are perfectly rigid, all deformation takes place in the fault zones and at the block base in contact with the underlying medium. Relative block displacements take place along the fault zones. This assumption is justified by the fact that for the lithosphere the effective elastic moduli of the fault zones are significantly smaller than those within the blocks. Block motion is defined so that the system is in a quasistatic equilibrium state. The interaction of blocks along the fault zones is viscous-elastic ("normal state") while the ratio of the stress to the pressure remains below a certain strength level. When the critical level is exceeded in some part of a fault zone, a stress-drop ("failure") occurs (in accordance with the dry friction model), possibly causing failure in other parts of the fault zones. These failures produce earthquakes. Immediately after the earthquake and for some time after, the affected parts of the fault zones are in a state of creep. This state differs from the normal state because of a faster growth of inelastic displacements, lasting until the stress falls below some other level. This numerical simulation gives rise to a synthetic earthquake catalogue.

The frequency-magnitude (FM) distribution (Ishimoto and Iida, 1939; Gutenberg and Richter, 1944) is described by the relation

$$\log_{10} N = a - bM, \quad (1)$$

where  $N$  is the cumulative number of earthquakes having magnitudes not less than  $M$ . The value of  $a$  in relation (1) characterises the total number of earthquakes while the value of  $b$  characterises size distribution of earthquakes. It has been shown that the value of  $b$  is not as constant and can vary in time and space. Variation of the  $b$ -value has been found for observable seismicity (e.g., Smith, 1986; Henderson et al., 1994; Ogata and Katsura, 1993; Amelung and King, 1997; Rotwain et al., 1997; Wiemer and Wyss, 1997; Wyss et al., 2000; Wyss and Wiemer, 2000; Burroughs and Tebbens, 2002), for synthetic seismicity generated in numerical models (e.g., Christensen and Olami, 1992; Narkunskaya and Shnirman, 1994; Amitrano, 2003; Zaliapin et al., 2003; Zöller et al., 2006) and for microfractures in laboratory samples (e.g., Rotwain et al., 1997; Amitrano, 2003). Theoretical models have been developed to explain temporal fluctuations in  $b$ -value (e.g., Main et al., 1989, 1992; Henderson et al., 1992).

The purpose of the present study is to analyze the behaviour of the  $b$ -value for the synthetic seismicity generated by the model of the block structure dynamics. We try to find difference in the  $b$ -value for periods preceding the largest earthquakes and periods that do not precede such earthquakes. A simple structure consisting of 4 square blocks is used for generating the synthetic earthquake catalogue. It follows from the analysis of the synthetic catalogue that the  $b$ -value is smaller for the periods preceding the largest earthquakes. The analysis of the earthquake catalogue of the Southern California gives similar results.

## 2 Description of the model

### 2.1 Block structure geometry

A layer with thickness  $H$ , limited by two horizontal planes is considered (Fig. 1), and a block-structure is a limited and simply-connected part of this layer. Each lateral boundary of the block-structure is defined by portions of parts of planes intersecting the layer. The subdivision of the structure into blocks is performed by planes intersecting the layer. The parts of these planes which are inside the block-structure and its lateral facets are called "fault planes."

The geometry of the block-structure is defined by the lines of intersection between the fault planes and the upper plane limiting the layer (these lines are called "faults"), and by the angles of dip of each fault plane. Three or more faults cannot have a common point on the upper plane, and a common point of two faults is called "vertex." The direction is specified for each fault and the angle of dip of the fault plane is

measured on the left of the fault. The positions of a vertex on the upper and the lower plane, limiting the layer, are connected by a segment (“rib”) of the line of intersection of the corresponding fault planes. The part of a fault plane between two ribs corresponding to successive vertices on the fault is called “segment.” The shape of the segment is a trapezium. The common parts of the block with the upper and lower planes are polygons, and the common part of the block with the lower plane is called “bottom.”

We assume that the block-structure is bordered by a confining medium, whose motion is prescribed on its continuous parts comprised between two ribs of the block-structure boundary. These parts of the confining medium are called “boundary blocks.”

## 2.2 Block movement

The movements of the boundaries of the block structure (the boundary blocks) and the medium underlying the blocks are assumed to be external force acting on the structure. The rates of these movements are considered to be horizontal and known. The movement of the underlying medium is specified separately for different blocks. Dimensionless time is used in the model, and all quantities containing time are referred to one unit of the dimensionless time. At each time the displacements of the blocks are determined in such a way that the structure is in a quasistatic equilibrium. All displacements of blocks are supposed to be infinitely small, compared with the block size. Therefore the geometry of the block structure does not change during the simulation and the structure does not move as a whole.

## 2.3 Interaction between blocks and the underlying medium

The elastic force which is due to the relative displacement of the block and the underlying medium, at some point of the block bottom, is assumed to be proportional to the difference between the total relative displacement vector and the vector of slippage (inelastic displacement) at the point. This force per unit area  $\mathbf{f}^u = (f_x^u, f_y^u)$  applied to the point with coordinates  $(X, Y)$ , at some time  $t$ , is defined by

$$f_x^u = K_u(x - x_u - (Y - Y_c)(\varphi - \varphi_u) - x_a), \quad (2)$$

$$f_y^u = K_u(y - y_u + (X - X_c)(\varphi - \varphi_u) - y_a). \quad (3)$$

where  $X_c, Y_c$  are the coordinates of the geometrical centre of the block bottom;  $(x_u, y_u)$  and  $\varphi_u$  are the translation vector and the angle of rotation (following the general convention, the positive direction of rotation is anticlockwise), around the geometrical centre of the block bottom, for the underlying medium at time  $t$ ;  $(x, y)$  and  $\varphi$  are the translation vector of the block and the angle of its rotation around the geometrical centre of its bottom at time  $t$ ;  $(x_a, y_a)$  is the inelastic displacement vector at the point  $(X, Y)$  at time  $t$ .

The evolution of the inelastic displacements at the point  $(X, Y)$  is described by the equations

$$\frac{dx_a}{dt} = W_u f_x^u, \quad \frac{dy_a}{dt} = W_u f_y^u. \quad (4)$$

The coefficients  $K_u$  and  $W_u$  in Eqs. (2–4) may be different for different blocks.

## 2.4 Interaction between the blocks along the fault planes

At the time  $t$ , in some point  $(X, Y)$  of the fault plane separating the blocks numbered  $i$  and  $j$  (the block numbered  $i$  is on the left and that numbered  $j$  is on the right of the fault) the components  $\Delta x$ ,  $\Delta y$  of the relative displacement of the blocks are defined by

$$\Delta x = x_i - x_j - (Y - Y_c^i)\varphi_i + (Y - Y_c^j)\varphi_j, \quad (5)$$

$$\Delta y = y_i - y_j + (X - X_c^i)\varphi_i - (X - X_c^j)\varphi_j. \quad (6)$$

where  $X_c^i, Y_c^i, X_c^j, Y_c^j$  are the coordinates of the geometrical centres of the block bottoms,  $(x_i, y_i)$ , and  $(x_j, y_j)$  are the translation vectors of the blocks, and  $\varphi_i, \varphi_j$  are the angles of rotation of the blocks around the geometrical centres of their bottoms, at time  $t$ .

In accordance with the assumption that the relative block displacements take place only along the fault planes; the displacements along the fault plane are connected with the horizontal relative displacement by

$$\Delta_t = e_x \Delta x + e_y \Delta y, \quad (7)$$

$$\Delta_l = \Delta_n / \cos \alpha, \text{ where } \Delta_n = e_x \Delta y - e_y \Delta x. \quad (8)$$

That is the displacements along the fault plane are projected on the horizontal plane. Here  $\Delta_t, \Delta_l$  are the displacements along the fault plane parallel ( $\Delta_t$ ) and normal ( $\Delta_l$ ) to the fault line on the upper plane,  $(e_x, e_y)$  is the unit vector along the fault line on the upper plane,  $\alpha$  is the dip angle of the fault plane, and  $\Delta_n$  is the horizontal displacement, normal to the fault line on the upper plane.

The elastic force per unit area  $\mathbf{f} = (f_t, f_l)$  acting along the fault plane at the point  $(X, Y)$  is defined by

$$f_t = K(\Delta_t - \delta_t), \quad (9)$$

$$f_l = K(\Delta_l - \delta_l). \quad (10)$$

Here  $\delta_t, \delta_l$  are inelastic displacements along the fault plane at the point  $(X, Y)$  at time  $t$ , parallel ( $\delta_t$ ) and normal ( $\delta_l$ ) to the fault line on the upper plane. The evolution of the inelastic displacement at the point  $(X, Y)$  is described by the equations

$$\frac{d\delta_t}{dt} = W f_t, \quad \frac{d\delta_l}{dt} = W f_l. \quad (11)$$

The coefficients  $K$  and  $W$  in Eqs. (9–11) are, respectively, proportional to the shear modulus and inversely proportional

to the viscous coefficient of the fault zone. The values of  $K$  and  $W$  can be different for different faults.

In addition to the elastic force, there is the reaction force which is normal to the fault plane; the work done by this force is zero, because all relative movements are tangent to the fault plane. The elastic energy per unit area at the point  $(X, Y)$  is equal to

$$e = (f_t(\Delta_t - \delta_t) + f_l(\Delta_l - \delta_l))/2. \quad (12)$$

From Eqs. (7), (8) and (12) the horizontal component of the elastic force per unit area, normal to the fault line on the upper plane,  $f_n$  can be written as:

$$f_n = \frac{\partial e}{\partial \Delta_n} = \frac{f_l}{\cos \alpha} \quad (13)$$

It follows from Eq. (13) that the total force acting at the point of the fault plane is horizontal if there is the reaction force, which is normal to the fault plane and its magnitude per unit area is equal to

$$p_0 = f_l \tan \alpha. \quad (14)$$

We introduce the reaction force Eq. (14) and therefore there are not vertical components of forces acting on the blocks and there are not vertical displacements of blocks.

Equations (5) and (6) are valid for the boundary faults too. In this case one of the blocks separated by the fault is the boundary block. The movement of these blocks is described by their translation and rotation around the origin of coordinates. Therefore the coordinates of the geometrical centre of the block bottom in Eqs. (5) and (6) are zero for the boundary block. For example, if the block numbered  $j$  is a boundary block, then  $X_c^j = Y_c^j = 0$  in Eqs. (5) and (6).

## 2.5 Equilibrium equations

The components of the translation vectors of the blocks and the angles of their rotation around the geometrical centres of the bottoms are found from the condition that the total force and the total moment of forces acting on each block are equal to zero. This is the condition of quasi-static equilibrium of the system and at the same time the condition of minimum energy. The forces arising from the specified movements of the underlying medium and of the boundaries of the block-structure are considered only in the equilibrium equations. In fact it is assumed that the action of all other forces (gravity, etc.) on the block-structure is balanced and does not cause displacements of the blocks.

In accordance with Eqs. (2), (3), (5–10) and (13) the dependence of the forces, acting on the blocks, on the translation vectors of the blocks and the angles of their rotations is linear. Therefore the system of equations which describes the equilibrium is linear one and has the following form

$$\mathbf{A}\mathbf{z} = \mathbf{b} \quad (15)$$

where the components of the unknown vector  $\mathbf{z}=(z_1, z_2, \dots, z_{3n})$  are the components of the translation vectors of the blocks and the angles of their rotation around the geometrical centres of the bottoms ( $n$  is the number of blocks), i.e.  $z_{3m-2}=x_m$ ,  $z_{3m-1}=y_m$ ,  $z_{3m}=q_m$  ( $m$  is the number of the block,  $m=1, 2, \dots, n$ ).

The matrix  $\mathbf{A}$  does not depend on time and its elements are defined from Eqs. (2), (3), (5–10) and (13). The moment of the forces acting on a block is calculated relative to the geometrical centre of its bottom. The expressions for the elements of the matrix  $\mathbf{A}$  contain integrals over the surfaces of the fault segments and of the block bottoms. Each integral is replaced by a finite sum, in accordance with the space discretization described in Sect. 2.6. The components of the vector  $\mathbf{b}$  are defined from Eqs. (2), (3), (5–10) and (13) as well. They depend on time, explicitly, because of the movements of the underlying medium and of the block-structure boundaries and, implicitly, because of the inelastic displacements.

## 2.6 Scheme of simulation

Formulas given above define the stress and the evolution of the inelastic displacements at points of fault zones and of block bottoms. To carry out the numerical simulation of block structure dynamics discretization of these plane surfaces is required. The discretization is defined by parameter  $\varepsilon$  and applied to fault segments and block bottoms as follows.

Each fault segment is a trapezoid with bases  $a$  and  $b$  and height  $h=H/\sin \alpha$  where  $H$  is the thickness of the layer, and  $\alpha$  is the dip angle of the fault plane. We determine the values

$$n_1 = \text{ENTIRE}(h/\varepsilon) + 1, \text{ and}$$

$$n_2 = \text{ENTIRE}(\max(a, b)/\varepsilon) + 1,$$

and divide the trapezoid into  $n_1 n_2$  small trapezoids by two groups of segments inside it; there are  $n_1-1$  segments parallel to the trapezoid bases and spaced at intervals  $h/n_1$ , and  $n_2-1$  segments connecting the points spaced by intervals of  $a/n_2$  and  $b/n_2$ , respectively, on the two bases. Small trapezoids obtained in this way are called “cells.” The coordinates  $X$ ,  $Y$  in Eqs. (5) and (6) and the inelastic displacements  $\delta_t$ ,  $\delta_l$  in Eqs. (9) and (10) are supposed to be the same for all the points of a cell and are considered average values over the cell. When introduced in Eqs. (5–10), (13), and (14), they yield the average (over the cell) of the elastic and reaction forces per unit area. The forces acting on a cell are obtained by multiplying the average forces per unit area by the area of the cell. The bottom of a block is a polygon. Prior to discretization, it is divided into trapezoids (triangles) by segments passing through its vertices and parallel to the  $Y$  axis. The discretization of these trapezoids (triangles) is performed in the same way as for fault segments.

The state of the block structure is considered at discrete time  $t_i=t_0 + i \Delta t$  where  $t_0$  is the initial time and  $i = 1, 2, \dots$ .

**Table 1.** Notations used in the paper and values of the parameters of the model of block structure dynamics

Parameters of the model of block structure dynamics	
Thickness of the layer	$H=20$ km
Difference between the lithostatic and the hydrostatic pressure in formula (16)	$P=2$ Kbars
Parameters for time and space discretization	$\Delta t=0.001$ , $\varepsilon=2.5$ km
Parameters of the block bottoms in Eqs. (2–4) (the same values for all blocks)	$K_u=1$ bar/cm, $W_u=0.05$ cm/bars
Dip angle of a fault plane (the same value for all faults)	$\alpha = 85^\circ$
Parameters of the fault planes in Eqs. (9–11) (the same values for all faults)	$K=1$ bar/cm, $W=0.05$ cm/bars, $W_s=10$ cm/bars
Levels of $\kappa$ Eq. (16) used for the determination of earthquakes and creep (the same values for all faults)	$B=0.1$ , $H_f=0.085$ , $H_s=0.07$
Parameters for determination of strong earthquakes, D- and N-periods, and b-value estimates	
Magnitude cut-off that defines strong earthquakes	$M_0$
Parameters used for determination of D- and N-periods	$\Delta_D$ , $\Delta_X$
Lower magnitude threshold for b-value estimates	$M_t$

The transition from the state at  $t_i$  to the state at  $t_{i+1}$  is made as follows: (i) new values of the inelastic displacements  $x_a$ ,  $y_a$ ,  $\delta_t$ ,  $\delta_l$  are calculated from Eqs. (4) and (11); (ii) the translation vectors and the rotation angles at  $t_{i+1}$  are calculated for the boundary blocks and the underlying medium; (iii) the components of  $\mathbf{b}$  in Eq. (15) are calculated, and these equations are used to define the translation vectors and the angles of rotation for the blocks.

## 2.7 Earthquake and creep

Earthquakes are simulated in accordance with the dry friction model. Let us introduce the quantity

$$\kappa = \frac{|f|}{P - p_0} \quad (16)$$

where  $\mathbf{f}=(f_t, f_l)$  is the elastic stress given by Eqs. (9) and (10);  $P$  is assumed equal for all the faults and can be interpreted as the difference between the lithostatic (due to gravity) and the hydrostatic pressure,  $p_0$ , given by Eq. (14), is the reaction force per unit area. The value of  $P$  reflects the average effective pressure in fault zones, and the difference  $P - p_0$  is the actual pressure for each cell.

Three following values of  $\kappa$  are assigned to each fault plane:  $B > H_f \geq H_s$ . If, at some time  $t_i$ , the value of  $\kappa$  in any cell of a fault segment reaches the level  $B$ , a failure ("earthquake") occurs (it is assumed that the initial conditions for the model satisfy the inequality  $\kappa < B$  for all cells of fault segments). The failure is considered slippage during which the inelastic displacements  $\delta_t$  and  $\delta_l$  in this cell change abruptly to reduce the value of  $\kappa$  to the level  $H_f$ . The level  $H_s$  is used in determination of the period of the creep state as described below.

After calculating the new values of the inelastic displacements for all the failed cells, step (iii) of the scheme of simulation (Sect. 2.6) is repeated with the same values of the absolute displacements and rotations of the boundary blocks and the underlying medium. If after that  $\kappa > B$  for some cell(s) of the fault segments, the inelastic displacements are recalculated for this cell(s), step (iii) of the scheme of simulation

is repeated and so on. When  $\kappa < B$  for all cells the state of the block structure at time  $t_{i+1}$  is determined in the ordinary way.

The cells belonging to the same fault plane, in which failure occurs at the same time, form a single earthquake. The magnitude of the earthquake is calculated from

$$M = 0.98 \log_{10} S + 3.93, \quad (17)$$

where  $S$  is the sum of the areas of the cells (in  $\text{km}^2$ ) forming the earthquake. The constants in Eq. (17) are specified in accordance with Utsu and Seki (1954).

It is assumed that the cells in which a failure has occurred are in the creep state immediately after the earthquake. This means that the parameter  $W_s$  ( $W_s > W$ ) is used instead of  $W$  for these cells in Eq. (11) to describe the evolution of inelastic displacements;  $W_s$  may be different for different faults. After each earthquake, a cell is in the creep state as long as  $\kappa > H_s$ , whereas when  $\kappa \leq H_s$  the cell returns to the normal state and henceforth the parameter  $W$  is used in Eq. (11) for this cell.

## 3 Block structure under consideration and a catalogue of synthetic earthquakes

The structure under consideration and its faults on the upper plane are shown in Fig. 2. Six faults (four of them are boundary faults) form a square with a side of 320 km divided into four smaller squares. Values of the model parameters are given in Table 1. The medium underlying all blocks of the structures does not move. The boundary movement is a translational movement at a velocity of 10 cm per unit dimensionless time. The directions of the velocity vectors are shown in Fig. 2. The angle between the velocity vector and the proper side of the square outlining a structure is  $10^\circ$ .

Numerical simulation of dynamics for the block structure under consideration was carried out for a period of 1000 dimensionless time units starting from the initial zero condition. The synthetic catalogue, which was analysed, contains earthquakes that occurred during the last 800 units of the simulation. The first 200 units were not considered to exclude

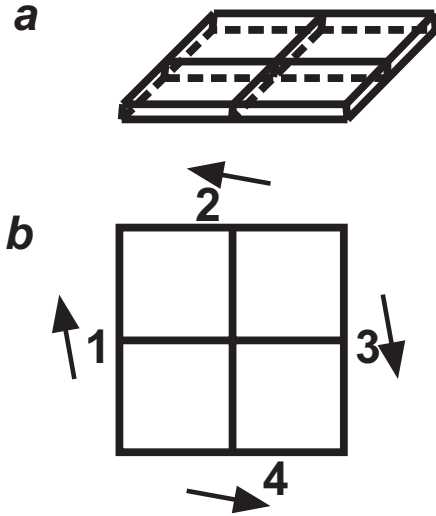


**Fig. 2.** The structure under consideration (a) and the scheme of its faults on the upper plane (b). The arrows show the vectors of velocities of boundaries, 1-4 are numbers of boundary sides of the structure.

the period that is needed in the model for quasi-stabilization of the stresses after starting the simulation from the initial zero conditions. The catalogue contains 41 788 events in the magnitude interval from 4.65 to 7.58. The FM plots are given in Fig. 3. They show the number of earthquakes with magnitude  $M$  (green bars) and the number of earthquakes with magnitude not less than  $M$  brown curve (cumulative FM plot).

## 4 Analysis of the synthetic catalogue

### 4.1 Definition of $D$ - and $N$ -periods

We try to find difference in the behaviour of background synthetic seismicity during the time intervals preceding strong earthquakes ( $D$ -periods) and time intervals that do not precede strong earthquakes ( $N$ -periods). Strong earthquakes are earthquakes with magnitude  $M \geq M_0$  where  $M_0$  is certain threshold.

We consider the following definition of  $D$ - and  $N$ -periods. Let  $T_1, T_2, \dots$  moments of strong events ( $T_{i+1} > T_i$ ). We use two parameters  $\Delta_D > 0$  and  $\Delta_X \geq 0$  and separate each interval  $[T_i, T_{i+1}]$  between two consecutive strong events into three non-intersecting intervals:  $D$ -interval,  $[T_{i+1} - \Delta_D, T_{i+1})$ ;  $X$ -interval,  $(T_i, T_i + \Delta_X)$ ; and  $N$ -interval,  $[T_i + \Delta_X, T_{i+1} - \Delta_D)$ . If  $T_{i+1} - T_i \leq \Delta_D$  then the whole interval  $(T_i, T_{i+1})$  is considered as  $D$ -interval. If  $\Delta_D < T_{i+1} - T_i \leq \Delta_D + \Delta_X$  then the interval  $(T_i, T_{i+1})$  is separated into  $D$ - and  $X$ -intervals only without  $N$ -interval, and  $X$ -interval in this case is  $(T_i, T_{i+1} - \Delta_D)$ .  $D$ -period is a combination of all  $D$ -intervals determined by this way and  $N$ -period is a combination of all

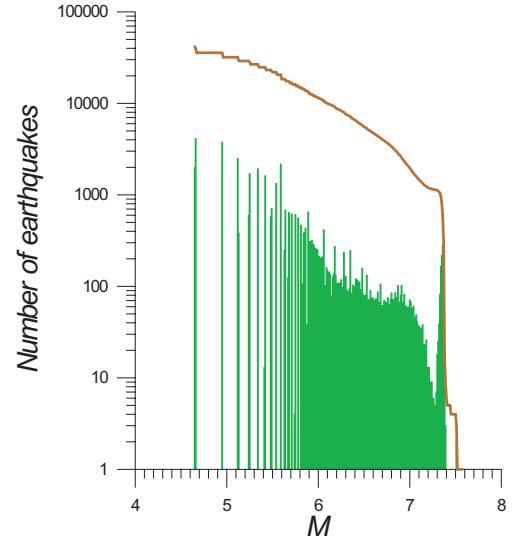


**Fig. 3.** Frequency-magnitude plots for the whole synthetic earthquake catalogue. Dependence of the number of earthquakes on the magnitude is shown by green bars while cumulative FM plot (the number of earthquakes with magnitude not less than  $M$ ) is shown by brown curve.

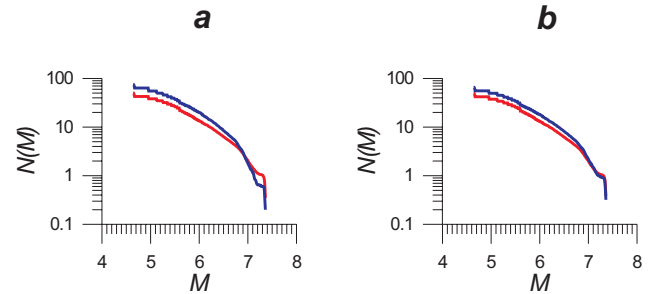


**Fig. 4.** Cumulative FM plots referred to one unit of dimensionless time constructed separately for  $D$ - and  $N$ -periods for the synthetic earthquake catalogue of the whole structure ( $N(M)$  is the number of earthquakes with magnitude not less than  $M$ ): red curves concern events occurred during  $D$ -period, blue curves – during  $N$ -period.  $D$ - and  $N$ -periods are determined with  $M_0 = 7.37$ ,  $\Delta_D = \Delta_X = 5$  (a) and  $\Delta_D = \Delta_X = 3$  (b).

$N$ -intervals.  $X$ -intervals are introduced to exclude intervals when the background seismicity is subjected to a strong event occurred before.

The behaviour of the background synthetic seismicity is characterized using the description of the FM distribution as given in Eq. (1) for earthquakes with magnitude  $M < M_0$ . The FM distributions are obtained separately for  $D$ - and  $N$ -periods. These two distributions and their description are then compared.

**Table 2.** Estimates of  $b$ -values of FM relations obtained separately for  $D$ - and  $N$ -periods for the whole structure,  $M_0=7.37$ ; uncertainty limits of the estimated  $b$ -value are given for the confidence probability 0.95.

Parameters for determination of $D$ - and $N$ -periods	$b^D(M_t)$	$b^N(M_t)$	$b^N(M_t) - b^D(M_t)$
$M_t=5.5$			
$\Delta_D = \Delta_X=5$ (Fig. 4a)	$0.6704 \pm 0.0078$	$0.6854 \pm 0.0244$	0.0150
$\Delta_D = \Delta_X=3$ (Fig. 4b)	$0.6694 \pm 0.0087$	$0.6731 \pm 0.0175$	0.0037
$M_t=6.0$			
$\Delta_D = \Delta_X=5$ (Fig. 4a)	$0.7893 \pm 0.0117$	$0.8951 \pm 0.0427$	0.1058
$\Delta_D = \Delta_X=3$ (Fig. 4b)	$0.7853 \pm 0.0129$	$0.8416 \pm 0.0285$	0.0563

#### 4.2 Quantitative measure of the difference between FM distributions

If a magnitude range  $M \geq M_t$  is considered then the  $b$ -value of FM plot in this magnitude range can be estimated as follows (Aki, 1965)

$$\hat{b}(M_t) = \frac{N(M_t)}{\ln 10 \sum_{M_i \geq M_t} (M_i - M_t)} \quad (18)$$

where  $N(M_t)$  is the number of earthquakes in the considered part of a catalogue with magnitude not less than  $M_t$ ,  $M_i$  – magnitudes of these earthquakes. Equation (18) gives a maximum-likelihood estimate of the  $b$ -value and is used to estimate the  $b$ -values separately for  $D$ - and  $N$ -periods ( $b^D(M_t)$  and  $b^N(M_t)$  respectively) determined in the catalogue considered above. The difference between  $b^D(M_t)$  and  $b^N(M_t)$  is used as a measure of the distinction between FM distributions obtained for  $D$ - and  $N$ -periods

#### 4.3 Analysis of the whole structure

The number of earthquakes versus the magnitude (Fig. 3) has an explicit local maximum in the magnitude range between 7.3 and 7.4. This maximum is attained at  $M=7.37$ . Accordingly to the definition of the magnitude in the model and geometrical sizes of the structure under consideration this value corresponds to an earthquake that covers completely one segment of a fault plane (in the structure under consideration all segments of the fault planes have approximately the same square). This value has been preliminary taken as the magnitude cut-off that defines strong earthquakes, i.e.  $M_0=7.37$ .

Figure 4 shows cumulative FM plots constructed separately for  $D$ - and  $N$ -periods determined by using the definition given above (Sect. 4.1) with  $\Delta_D=\Delta_X=5$  (Fig. 4a) and  $\Delta_D=\Delta_X=3$  (Fig. 4b). Values of  $\Delta_D$  and  $\Delta_X$  are given in units of the dimensionless time. The number of events used for constructing the plots is referred to one unit of dimensionless time, i.e. the numbers of earthquakes for different magnitude ranges are divided on duration (in units of dimensionless time) of  $D$ - and  $N$ -periods respectively. Comparing the plots one can see difference between FM plots for  $D$ - and

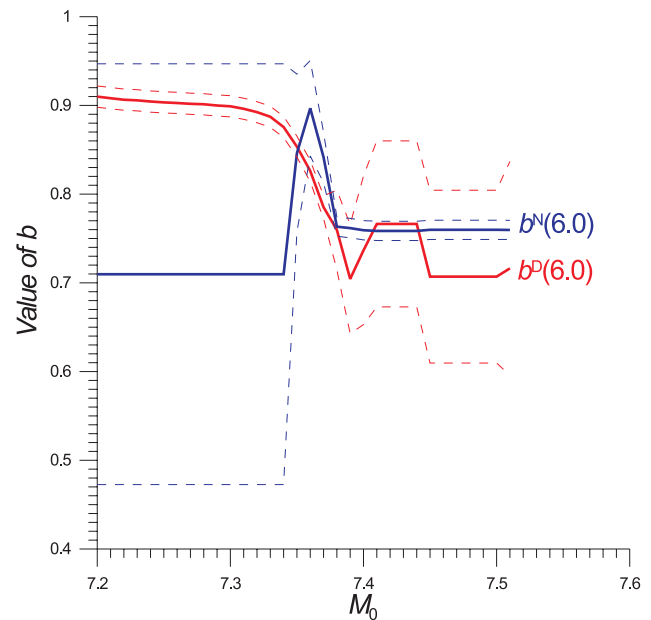


**Fig. 5.** Dependence of  $b^D(6.0)$  (red curve) and  $b^N(6.0)$  (blue curve) on  $M_0$ ;  $b^D(6.0)$  and  $b^N(6.0)$  are calculated for the synthetic earthquake catalogue of the whole structure using Eq. (18) for  $D$ - and  $N$ -periods respectively.  $D$ - and  $N$ -periods are determined with a current value of  $M_0$  and  $\Delta_D=\Delta_X=3$ . Dotted curves show limits of the confidence interval for the confidence probability 0.95.

$N$ -periods. The plots for  $D$ -period demonstrate considerable deficiency of the events with small magnitudes in comparison with the plots for  $N$ -period. In the range of large magnitudes ( $M > 7.0$ ) the incidence of the plot for  $N$ -period obtained with  $\Delta_D=\Delta_X=5$  (Fig. 4a) is appreciably greater than that for  $D$ -period. The similar phenomenon was found formerly for observed seismicity and in models (e.g., Narkunskaya and Shnirman, 1994; Rotwain et al., 1997; Zaliapin et al., 2003). Results of calculation of the  $b$ -values separately for  $D$ - and  $N$ -periods ( $b^D(M_t)$  and  $b^N(M_t)$ ) by means of Eq. (18) with two values of  $M_t$  (5.5 and 6.0) are given in Table 2. Uncertainty (confidence) limits of the estimated  $b$ -value are calculated here and below in accordance with



**Table 3.** Estimates of  $b$ -values of FM relations obtained separately for  $D$ - and  $N$ -periods for the seismicity of the Southern California,  $M_0=6.4$ ; uncertainty limits of the estimated  $b$ -value are given for the confidence probability 0.95.

Parameters for determination of $D$ - and $N$ -periods	$b^D(M_t)$	$b^N(M_t)$	$b^N(M_t) - b^D(M_t)$
$M_t=4.5$			
$\Delta_D=\Delta_X=3$ years (Fig. 9a)	$1.1332\pm 0.0569$	$1.4372\pm 0.1872$	0.3040
$\Delta_D=\Delta_X=2$ years (Fig. 9b)	$1.1204\pm 0.0615$	$1.3517\pm 0.1179$	0.2313
$M_t=5.0$			
$\Delta_D=\Delta_X=3$ years (Fig. 9a)	$1.2289\pm 0.0933$	$1.5986\pm 0.4461$	0.3697
$\Delta_D=\Delta_X=2$ years (Fig. 9b)	$1.1436\pm 0.0929$	$1.5511\pm 0.2568$	0.4075

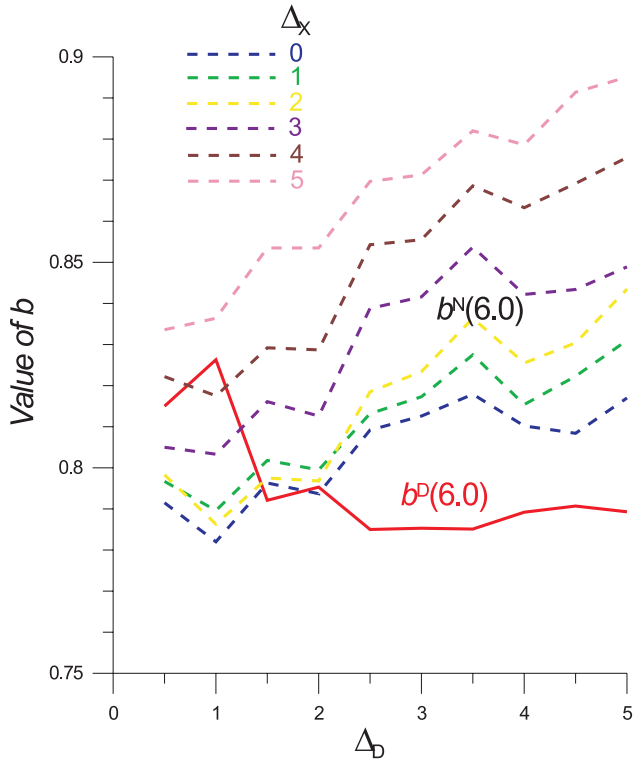


**Fig. 6.** Dependence of  $b^D(6.0)$  (solid red curve) and  $b^N(6.0)$  (dotted curves) on  $\Delta_D$  and  $\Delta_X$ ;  $b^D(6.0)$  and  $b^N(6.0)$  are calculated for the synthetic earthquake catalogue of the whole structure using (18) for  $D$ - and  $N$ -periods respectively.  $D$ - and  $N$ -periods are determined with  $M_0=7.37$  and current values of  $\Delta_D$  and  $\Delta_X$ . Note that  $D$ -period and therefore  $b^D(M_t)$  do not depend on  $\Delta_X$ .

Molchan and Podgaetskaya (1973). One can see that in all cases  $b^D(M_t) < b^N(M_t)$  but difference  $b^N(M_t) - b^D(M_t)$  is larger than the uncertainty limits of the estimated  $b$ -value only if  $M_t=6.0$ .

To check the robustness and the stability of the results with respect to parameters that determine strong earthquakes ( $M_0$ ) and  $D$ - and  $N$ -periods ( $\Delta_D$  and  $\Delta_X$ )  $b^D(6.0)$  and  $b^N(6.0)$  were calculated with different values of these parameters. Figure 5 shows the dependence of  $b^D(6.0)$  and  $b^N(6.0)$  on

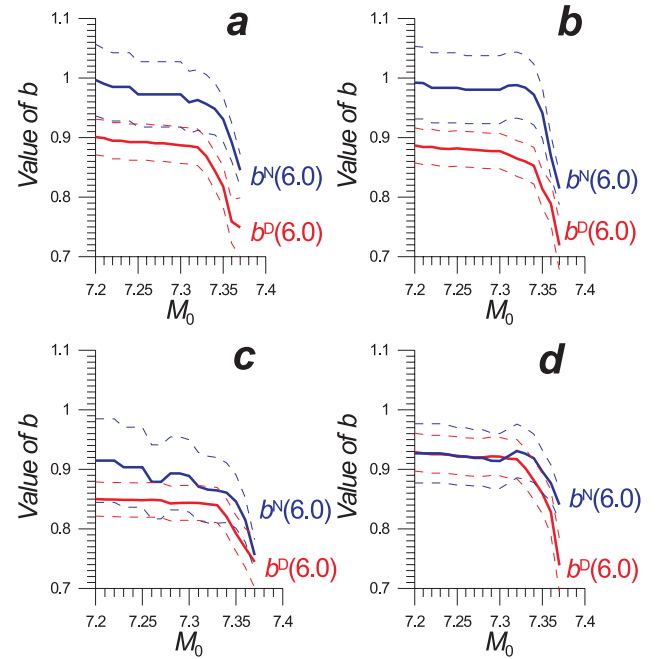


**Fig. 7.** Dependence of  $b^D(6.0)$  (red curves) and  $b^N(6.0)$  (blue curves) on  $M_0$ ;  $b^D(6.0)$  and  $b^N(6.0)$  are calculated for the synthetic earthquake catalogues of the boundary fault planes 1 (a), 2 (b), 3 (c), and 4 (d) using Eq. (18) for  $D$ - and  $N$ -periods respectively.  $D$ - and  $N$ -periods are determined with a current value of  $M_0$  and  $\Delta_D=\Delta_X=3$ . Dotted curves show limits of the confidence interval for the confidence probability 0.95.

$M_0$  when  $\Delta_D=\Delta_X=3$  and Fig. 6 shows their dependence on  $\Delta_D$  and  $\Delta_X$  when  $M_0=7.37$ . Figure 6 demonstrates stability of the result to variation of values  $\Delta_D$  and  $\Delta_X$  when  $\Delta_D > 2$  but as follows from Fig. 5 the relationship  $b^D(6.0) < b^N(6.0)$  is valid in a narrow magnitude range about  $M_0=7.37$ . The last can be explained as follows. By definition (Sect. 2.7) the synthetic earthquakes are formed from cells belonging to the same fault plane. Behaviour of the background seismicity changes before a strong earthquake mainly on the same fault plane where this strong earthquake occurs. When the background seismicity of the whole structure is considered

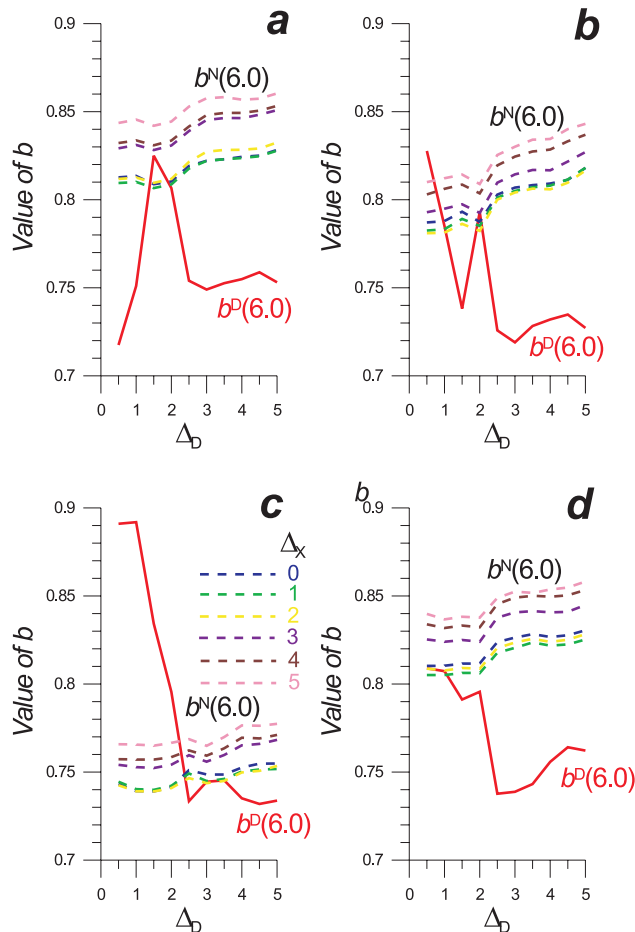


**Fig. 8.** Dependence of  $b^D(6.0)$  (solid red curve) and  $b^N(6.0)$  (dotted curves) on  $\Delta_D$  and  $\Delta_X$ ;  $b^D(6.0)$  and  $b^N(6.0)$  are calculated for the synthetic earthquake catalogue of the boundary fault planes 1 (a), 2 (b), 3 (c), and 4 (d) using Eq. (18) for  $D$ - and  $N$ -periods respectively.  $D$ - and  $N$ -periods are determined with  $M_0=7.37$  and current values of  $\Delta_D$  and  $\Delta_X$ . Note that  $D$ -period and therefore  $b^D(M_t)$  do not depend on  $\Delta_X$ .

periods preceding strong earthquakes for some fault planes are mixed with periods not preceding strong earthquakes for other faults and changes in the  $b$ -value before strong earthquakes are not seen. One can avoid this by considering the fault planes separately.

#### 4.4 Separate analysis of boundary fault planes

The strong earthquakes occur in boundary fault planes of the structure. These fault planes are marked 1–4 in Fig. 2. We considered separately catalogues of synthetic earthquakes occurred in different fault planes, and  $D$ - and  $N$ -periods were determined for each boundary fault plane accordingly to strong earthquakes occurred in it. The dependence of  $b^D(6.0)$  and  $b^N(6.0)$  on  $M_0$  when  $\Delta_D=\Delta_X=3$  is shown in Fig. 7 separately for different boundary fault planes.

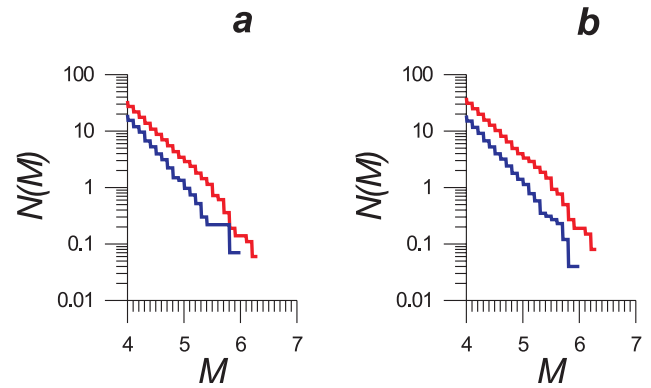


**Fig. 9.** Cumulative FM plots referred to one year constructed separately for  $D$ - and  $N$ -periods for the seismicity of the Southern California, 1932–2006 ( $N(M)$  is the number of earthquakes with magnitude not less than  $M$ ): red curves concern events occurred during  $D$ -period, blue curves – during  $N$ -period.  $D$ - and  $N$ -periods are determined with  $M_0=6.4$ ,  $\Delta_D=\Delta_X=3$  years (a) and  $\Delta_D=\Delta_X=2$  years (b).

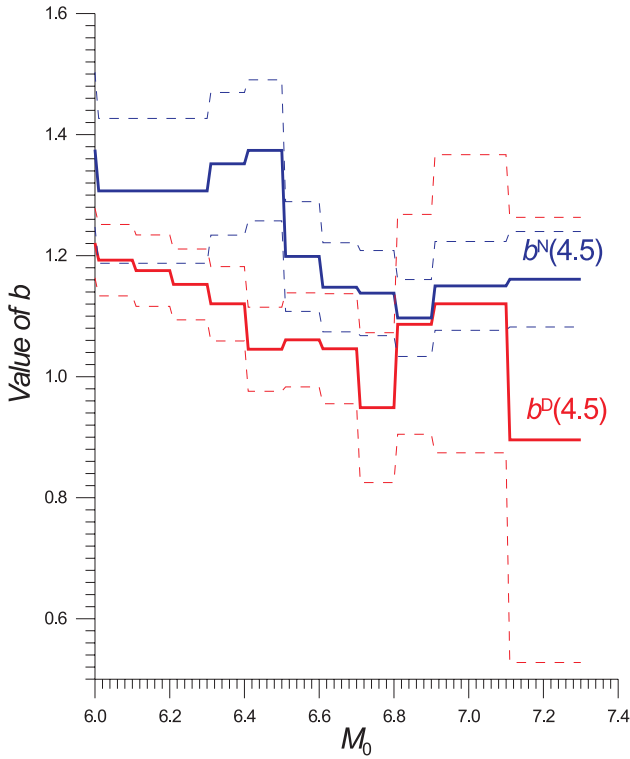
Comparing Figs. 5 and 7 one can see that for the fault planes 1 (Fig. 7a) and 2 (Fig. 7b) considered separately the magnitude range where  $b^D(6.0) < b^N(6.0)$  is essentially wider than in the case of the whole structure.

Figure 8 shows the dependence of  $b^D(6.0)$  and  $b^N(6.0)$  on  $\Delta_D$  and  $\Delta_X$  when  $M_0=7.37$ . One can see that if  $\Delta_D$  is large enough the relationship  $b^D(6.0) < b^N(6.0)$  is stable with regard to variations of  $\Delta_X$ . This figure does not change principally if another value of  $M_0$  is selected from the range (7.20, 7.37).

## 5 Analyses of seismicity of the Southern California

Seismicity of the Southern California has been analysed in the similar way as the synthetic seismicity obtained in the model. The data on seismicity of the Southern California have been taken from The Southern California Earthquake Data Centre (SCEDC) catalogue. It consists of hypocentral information for 1932 through the present. The information on catalogue completeness and data sources can be found at the web site (SCEDC).

Earthquakes with magnitude  $M \geq M_0=6.4$  are considered as strong events and earthquakes with  $4 \leq M < 6.4$  are analyzed as the background seismicity. Figure 9 shows cumulative FM plots referred to one year and constructed separately for  $D$ - and  $N$ -periods that were determined with  $\Delta_D=\Delta_X=3$  years (Fig. 9a) and  $\Delta_D=\Delta_X=2$  years (Fig. 9b). In the both cases one can see difference between the plots for  $D$ - and  $N$ -periods. Table 3 contains the  $b$ -values calculated separately for  $D$ - and  $N$ -periods by means of Eq. (18). As in the case of synthetic seismicity  $b^D(M_t)$  is less than  $b^N(M_t)$ . But when  $\Delta_D=\Delta_X=3$  years and  $M_t=5.0$  difference  $b^N(M_t)-b^D(M_t)$  is



**Fig. 10.** Dependence of  $b^D(4.5)$  (red curve) and  $b^N(4.5)$  (blue curve) on  $M_0$ ;  $b^D(4.5)$  and  $b^N(4.5)$  are calculated for the seismicity of the Southern California, 1932–2006 using Eq. (18) for  $D$ - and  $N$ -periods respectively.  $D$ - and  $N$ -periods are determined with a current value of  $M_0$  and  $\Delta_D = \Delta_X = 2$  years. Dotted curves show limits of the confidence interval for the confidence probability 0.95.

less than the uncertainty limits of the estimated  $b$ -value, and so,  $M_i = 4.5$  has been used in the further analysis.

The dependence of  $b^D(4.5)$  and  $b^N(4.5)$  on the values of parameter  $M_0$ ,  $\Delta_D$ , and  $\Delta_X$  is shown in Figs. 10 and 11. Figure 10 shows the dependence of  $b^D(4.5)$  and  $b^N(4.5)$  on  $M_0$  when  $\Delta_D = \Delta_X = 2$  years. One can see from this figure that  $b^D(4.5) < b^N(4.5)$  for all  $M_0 \geq 6.0$  but difference  $b^N(4.5) - b^D(4.5)$  exceeds the uncertainty limits of the estimated  $b$ -value only in a narrow magnitude range about  $M_0 = 6.4$ . Figure 11 shows the dependence of  $b^D(4.5)$  and  $b^N(4.5)$  on the values of  $\Delta_D$  and  $\Delta_X$  when  $M_0 = 6.4$  and demonstrates stability of the result to their variation when  $\Delta_D > 1$  year.

## 6 Discussion

The calculations made for the model of block structure dynamics show that  $b^D(6.0)$  decreases monotonically when the magnitude cut-off for strong earthquakes  $M_0$  increases from 7.2 to 7.37. This occurs both for the whole structure (Fig. 5) and for the separate fault planes (Fig. 7). In the case of the seismicity of the Southern California (Fig. 10)  $b^D(4.5)$  decreases also when  $M_0$  increases from 6.0 to 6.4. Possi-

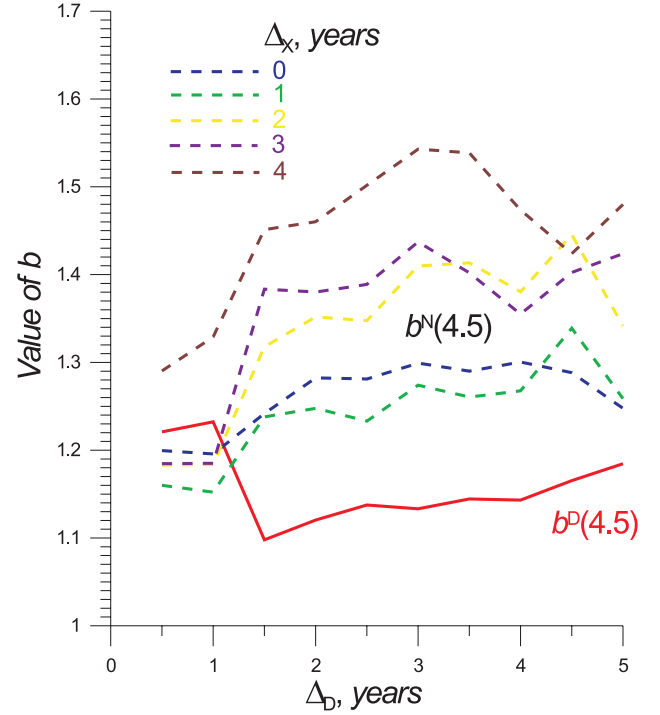


**Fig. 11.** Dependence of  $b^D(4.5)$  (solid red curve) and  $b^N(4.5)$  (dotted curves) on  $\Delta_D$  and  $\Delta_X$ ;  $b^D(4.5)$  and  $b^N(4.5)$  are calculated for the seismicity of the Southern California, 1932–2006 using Eq. (18) for  $D$ - and  $N$ -periods respectively.  $D$ - and  $N$ -periods are determined with  $M_0 = 6.4$  and current values of  $\Delta_D$  and  $\Delta_X$ . Note that  $D$ -period and therefore  $b^D(M_i)$  do not depend on  $\Delta_X$ .

ble explanation of this is that the preparation of the larger earthquakes affects more (in terms of decreasing  $b$ -value) on the background seismicity. When the largest earthquakes ( $M_0 > 7.37$  for the model or  $M_0 > 6.4$  for the seismicity of the Southern California) are considered this dependence of  $b^D(M_i)$  on  $M_0$  does not occur. But in this case the number of strong earthquakes is small, duration of  $D$ -period is short, and the estimate of  $b$ -value is unreliable that is seen from the limits of the confidence interval of  $b^D(M_i)$  given in Figs. 5 and 10.

Comparing Figs. 5 and 7 one can see that when  $M_0 < 7.36$   $b^D(6.0) > b^N(6.0)$  for the whole structure (Fig. 5) while  $b^D(6.0) < b^N(6.0)$  for the fault planes 1–3 (Fig. 7a–c). This can be explained by the fact that in the case of the whole structure the number of strong earthquakes determined with the magnitude cut-off  $M_0 < 7.36$  is very large, accordingly  $N$ -period is very short, and the estimate of  $b$ -value is unreliable that is seen from the limits of the confidence interval of  $b^D(6.0)$  given in Fig. 5. Note that taking into account the limits of the confidence intervals given in Fig. 7 we can be sure that the inequality  $b^D(6.0) < b^N(6.0)$  exists indeed only for the fault planes 1 and 2 (Fig. 7a, b). The difference between the fault planes 1 and 2 on the one hand and the fault planes 3

and 4 on the other hand that is seen in Fig. 7 demonstrates the complexity of the model under consideration. Depending on  $M_0$  of  $b^D(4.5)$  and  $b^N(4.5)$  for the seismicity of the Southern California (Fig. 10) looks like that of  $b^D(6.0)$  and  $b^N(6.0)$  for the separate fault planes of the block structure (Fig. 7) and  $b^D(4.5) < b^N(4.5)$  for the seismicity of the Southern California as well as  $b^D(6.0) < b^N(6.0)$  for the fault planes 1–3. This likeness between the Southern California and the separate fault planes can be possibly explained by presence in the Southern California of the dominating fault structure – the San Andreas Fault.

A model has been presented by Main et al. (1989), which can explain the temporal fluctuations in the  $b$ -value and predicts during a period before a large earthquake two minima in the  $b$ -value, separated by a temporary maximum. One can see the similar feature in dependence of  $b^D(6.0)$  on  $\Delta_D$  in the cases of the whole structure (Fig. 6, minima at  $\Delta_D=0.5$  and 2.5 and maximum at  $\Delta_D=1$ ) and of individual fault planes. It is rather distinct for fault plane 1 (Fig. 8a, minima at  $\Delta_D=0.5$  and 3 and maximum at  $\Delta_D=1.5$ ) and fault plane 2 (Fig. 8b, minima at  $\Delta_D=1.5$  and 3 and maximum at  $\Delta_D=2$ ) and not so distinct for fault plane 3 (Fig. 8c, minima at  $\Delta_D=2.5$  and 4.5 and maximum at  $\Delta_D=3-3.5$ ) and fault plane 4 (Fig. 8d, minima at  $\Delta_D=1.5$  and 2.5 and maximum at  $\Delta_D=2$ ). Dependence of  $b^D(4.5)$  on  $\Delta_D$  for the seismicity of the Southern California (Fig. 11) has also two minima at  $\Delta_D=0.5$  and 1.5 years and maximum at  $\Delta_D=1$  year.

## 7 Conclusions

The phenomenon of transformation of FM plot before strong earthquakes identified here in the model of block structure dynamics and observed in the seismicity of the Southern California demonstrates redistribution of sizes of earthquakes before a strong one: decreasing of the  $b$ -value means that the number of small earthquakes decreases while the number of large earthquakes increases. The possibility to use this phenomenon for earthquake prediction is discussed, e.g. by Eneva and Ben-Zion (1997) who consider a parameter “magnitude ratio” (ratio of numbers of events in two different magnitude ranges). It is also reflected by one of functions on an earthquake flow used in earthquake prediction algorithm M8 (Keilis-Borok and Kossobokov, 1990).

The model of block structure dynamics allows to reproduce different configurations of blocks and faults and to specify various movements of the underlying medium and boundary blocks and some features of the fault zones that are reflected by parameters  $K$ ,  $W$ ,  $W_s$ ,  $B$ ,  $H_f$ , and  $H_s$ . Detecting of the transformation of FM plot before strong earthquakes in the model gives possibility to study how the manifestation of this phenomenon depends on the block structure geometry, the movements specified, and the features of the fault zones.

**Acknowledgements.** This work was supported by the EC Project “Extreme events: Causes and consequences (E2-C2), Contract No 12975 (NEST).”

Edited by: H. Rust

Reviewed by: M. Baiesi and three other anonymous referees

## References

- Aki, K.: Maximum likelihood estimate of  $b$  in formula  $\log N=a-bM$  and its confidence limits, *Bull. Earthquake Res. Inst. Univ. Tokyo*, 43, 237–239, 1965.
- Allègre, C. J., Le Mouél, J.-L., and Provost, A.: Scaling rules in rock fracture and possible implications for earthquake prediction, *Nature*, 297, 47–49, 1982.
- Allègre, C. J., Le Mouél, J.-L., Chau, H. D., and Narteau, C.: Scaling organization of fracture tectonics (SOFT) and earthquake mechanism, *Phys. Earth Planet. Inter.*, 92, 215–233, 1995.
- Amelung, F. and King, G.: Earthquake scaling laws for creeping and noncreeping faults, *Geophys. Res. Lett.*, 24, 507–510, 1997.
- Amitrano, D.: Brittle-ductile transition and associated seismicity: Experimental and numerical studies and relationship with the  $b$  value, *J. Geophys. Res.*, 108, 2044, doi:10.1029/2001JB000680, 2003.
- Bak, P. and Tang, C.: Earthquakes as a self-organized critical phenomenon, *Geophys. Res. Lett.*, 94, 15 635–15 637, 1989.
- Barenblatt, G. I., Keilis-Borok, V. I., and Monin, A. S.: Filtration model of earthquake sequence, *Transactions (Doklady) Acad. Sci. SSSR*, 269, 831–834, 1983.
- Ben-Zion, Y. and Rice, J. R.: Earthquake failure sequence along a cellular fault zone in a three-dimensional elastic solid containing asperity and nonasperity regions, *J. Geophys. Res.*, 98, 14 109–14 131, 1993.
- Ben-Zion, Y. and Lyakhovsky, V.: Analysis of aftershocks in a lithospheric model with seismogenic zone governed by damage rheology, *Geophys. J. Int.*, 165, 197–210, 2006.
- Blanter, E. M., Shnirman, M. G., and Le Mouél, J.-L.: Hierarchical model of seismicity: Scaling and predictability, *Phys. Earth Planet. Inter.*, 103, 135–150, 1998.
- Burridge, R. and Knopoff, L.: Model and theoretical seismicity, *Bull. Seismol. Soc. Am.*, 57, 341–360, 1967.
- Burroughs, S. M. and Tebbens, S. F.: The upper-truncated power law applied to earthquake cumulative frequency-magnitude distributions: evidence for a time-independent scaling parameter, *Bull. Seismol. Soc. Am.*, 92, 2983–2993, 2002.
- Christensen, K. and Olami, Z.: Variation of the Gutenberg-Richter  $b$  values and nontrivial temporal correlations in a spring-block model for earthquakes, *J. Geophys. Res.*, 97, 8729–8735, 1992.
- Dieterich, J. H.: Time-dependent friction as a possible mechanism for aftershocks, *J. Geophys. Res.*, 77, 3771–3781, 1972.
- Dieterich, J. H.: A constitutive law for earthquake production and its application to earthquake clustering, *J. Geophys. Res.*, 99, 2601–2618, 1994.
- Eneva, M. and Ben-Zion, Y.: Techniques and parameters to analyze seismicity patterns associated with large earthquakes, *J. Geophys. Res.*, 102, 17 785–17 795, 1997.
- Fitzenz, D. D. and Miller, S. A.: A forward model for earthquake generation on interacting faults including tectonics, fluids, and stress transfer, *J. Geophys. Res.*, 106, 26 689–26 706, 2001.

- Gabrielov, A. M. and Keilis-Borok, V. I.: Patterns of stress corrosion: Geometry of the principal stresses, *Pure Appl. Geophys.*, 121, 477–494, 1983.
- Gabrielov, A. M., Levshina, T. A., and Rotwain, I. M.: Block model of earthquake sequence, *Phys. Earth and Planet. Inter.*, 61, 18–28, 1990.
- Gabrielov, A. M., Keilis-Borok, V. I., Zaliapin, I. V., and Newman, W. I.: Critical transitions in colliding cascades, *Phys. Rev. E*, 62, 237–249, 2000.
- Gutenberg, R. and Richter, C. F.: Frequency of earthquakes in California, *Bull. Seismol. Soc. Am.*, 34, 185–188, 1944.
- Ishimoto, M. and Iida, K.: Observations on earthquakes registered with the microseismograph constructed recently, *Bull. Earthquake Res. Inst. Univ. Tokyo*, 17, 443–478, 1939.
- Ismail-Zadeh A., Le Mouél, J.-L., Soloviev, A., Tapponnier, P., and Vorovieva, I.: Numerical modeling of crustal block-and-fault dynamics, earthquakes and slip rates in the Tibet-Himalayan region, *EPSL*, 258, 465–485, 2007.
- Ito, K. and Matsuzaki, M.: Earthquakes as self-organized critical phenomena, *J. Geophys. Res.*, 95, 6853–6860, 1990.
- Hainzl, S., Zöller, G., and Kurths, J.: Similar power laws for fore- and aftershock sequences in a spring-block model for earthquakes, *J. Geophys. Res.*, 104, 7243–7253, 1999.
- Henderson, J., Main, I., Meredith, P., and Sammonds, P.: The evolution of seismicity at Parkfield: observation, experiment and a fracture-mechanical interpretation, *J. Struct. Geol.*, 14, 905–913, 1992.
- Henderson, J., Main, I. G., Pearce, R. G., and Takeya, M.: Seismicity in north-eastern Brazil: fractal clustering and the evolution of the  $b$  value, *Geophys. J. Int.*, 116, 217–226, 1994.
- Keilis-Borok, V. I. and Kossobokov, V. G.: Premonitory activation of earthquake flow: algorithm M8, *Phys. Earth Planet. Inter.*, 61, 73–83, 1990.
- Keilis-Borok, V. I., Rotwain, I. M., and Soloviev, A. A.: Numerical modeling of block structure dynamics: dependence of a synthetic earthquake flow on the structure separateness and boundary movements, *J. Seismol.*, 1, 151–160, 1997.
- Main, I. G., Meredith, P. G., and Jones, C.: A reinterpretation of the precursory seismic  $b$ -value anomaly from fracture mechanics, *Geophys. J. Int.*, 96, 131–138, 1989.
- Main, I. G., Meredith, P. G., and Sammonds, P. R.: Temporal variations in seismic event rate and  $b$ -values from stress corrosion constitutive laws, *Tectonophysics*, 211, 233–246, 1992.
- Molchan, G. M. and Podgaetskaya, V. M.: Parameters of the global seismicity, I, in: *Computational and Statistical Methods of Seismic Data Interpretation*, edited by: Keilis-Borok, V. I., 44–66, Nauka, Moscow, 1973.
- Narkunskaya, G. S. and Shnirman, M. G.: On an algorithm of earthquake prediction, in: *Computational Seismology and Geodynamics*, Vol. 1, edited by: Chowdhury, D. K., 20–24, AGU, Washington, D.C., 1994.
- Nur, A. and Booker, J. R.: Aftershocks caused by pore fluid flow?, *Science*, 175, 885–887, 1972.
- Ogata, Y., and Katsura, K.: Analysis of temporal and spatial heterogeneity of magnitude frequency distribution inferred from earthquake catalogues, *Geophys. J. Int.*, 113, 727–738, 1993.
- Olami, Z., Feder, H. J. S., and Christensen, K.: Self-organized criticality in a continuous, nonconservative cellular automaton modeling earthquakes, *Phys. Rev. Lett.*, 68, 1244–1247, 1992.
- Robinson, R. and Benites, R.: Synthetic seismicity models for the Wellington region, New Zealand: Implications for temporal distribution of large events, *J. Geophys. Res.*, 101, 27 833–27 844, 1996.
- Robinson, R. and Benites, R.: Upgrading a synthetic seismicity model for more realistic fault ruptures, *Geophys. Res. Lett.*, 28, 1843–1846, 2001.
- Rotwain, I., Keilis-Borok, V., and Botvina, L.: Premonitory transformation of steel fracturing and seismicity, *Phys. Earth Planet. Inter.*, 101, 61–71, 1997.
- SCEDC: web site [http://www.data.scec.org/about/data\\_avail.html](http://www.data.scec.org/about/data_avail.html).
- Smith, W. D.: Evidence for precursory changes in the frequency-magnitude  $b$ -value, *Geophys. J. Int.*, 86, 815–838, 1986.
- Soloviev, A. and Ismail-Zadeh, A.: Models of dynamics of block-and-fault systems, in: *Nonlinear Dynamics of the Lithosphere and Earthquake Prediction*, edited by: Keilis-Borok, V. I. and Soloviev, A. A., 71–139, Springer-Verlag, Berlin-Heidelberg, 2003.
- Utsu, T. and Seki, A.: A relation between the area of aftershock region and the energy of main shock, *J. Seism. Soc. Japan*, 7, 233–240, 1954.
- Ward, S. N.: An application of synthetic seismicity in earthquake statistics: The Middle America Trench, *J. Geophys. Res.*, 97, 6675–6682, 1992.
- Ward, S. N.: San Francisco Bay Area earthquake simulation: A step toward a standard physical earthquake model, *Bull. Seismol. Soc. Am.*, 90, 370–386, 2000.
- Wiemer, S. and Wyss, M.: Mapping the frequency-magnitude distribution in asperities: An improved technique to calculate recurrence times?, *J. Geophys. Res.*, 102, 15 115–15 128, 1997.
- Wyss, M., Schorlemmer, D., and Wiemer, S.: Mapping asperities by minima of local recurrence time: San Jacinto-Elsinore fault zones, *J. Geophys. Res.*, 105, 7829–7844, 2000.
- Wyss, M. and Wiemer, S.: Change in the probability for earthquakes in Southern California due to the Landers magnitude 7.3 earthquake, *Science*, 290, 1334–1338, 2000.
- Zaliapin, I., Keilis-Borok, V., and Ghil, M.: A Boolean delay model of colliding cascades. II: Prediction of critical transitions, *J. Stat. Phys.*, 111, 839–861, 2003.
- Zhou, S., Johnston, S., Robinson, R., and Vere-Jones, D.: Tests of the precursory accelerating moment release model using a synthetic seismicity model for Wellington, New Zealand, *J. Geophys. Res.*, 111, B05308, doi:10.1029/2005JB003720, 2006.
- Zöller, G., Hainzl, S., Holschneider, M., and Ben-Zion, Y.: Aftershocks resulting from creeping sections in a heterogeneous fault, *Geophys. Res. Lett.*, 32, L03308, doi:10.1029/2004GL021871, 2005.
- Zöller, G., Hainzl, S., Ben-Zion, Y., and Holschneider, M.: Earthquake activity related to seismic cycles in a model for a heterogeneous strike-slip fault, *Tectonophysics*, 423, 137–145, 2006.